Journal of Materials Chemistry A

Accepted Manuscript

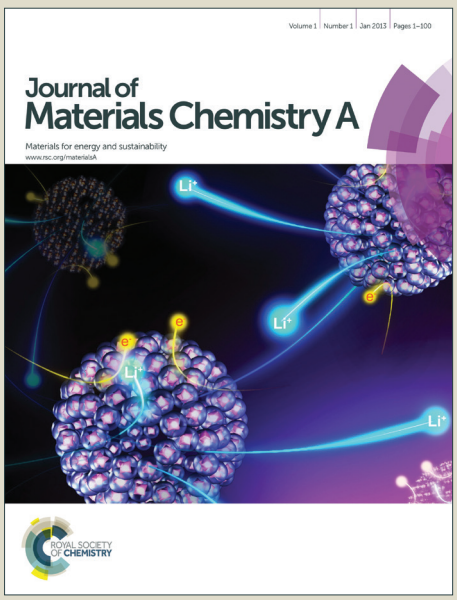

ROYAL SOCIETY OF CHEMISTRY

www.rsc.org/materialsA

Journal of Materials Chemistry A

Dynamic Article Links ►

Journal of Materials Chemistry A

Cite this: DOI: 10.1039/c0xx00000x

www.rsc.org/xxxxxx

PAPER

Nanocrystalline-Li_2FeSiO_4 Synthesized by Carbon Frameworks as Advanced Cathode Materials for Li-ion Batteries

Jinlong Yang, Xiaochun Kang, Lin Hu, Xue Gong and Shichun Mu*

Received (in XXX, XXX) Xth XXXXXXXXX 20XX, Accepted Xth XXXXXXXXX 20XX

DOI: 10.1039/b000000x

The $P2_1/n$ structure nanocrystalline-Li_2FeSiO_4 is prepared by a confinement effect of three-dimensional conductive carbon frameworks which is formed through a chelating reaction and subsequent pyrolysis. Benefit of enhanced electronic conductivity by carbon frameworks and Li-ion diffusion kinetics by nanocrystalline-Li_2FeSiO_4 architectures, the novel nanocomposite shows 1.28 Li-ion storage capacity (211.3 mAh g^{-1}) at 0.1C, corresponding to successive two steps of oxidation and reduction of $Fe^{2+}/Fe^{3+}/Fe^{4+}$. Furthermore, the discharge capacity is 189.8, 175.6, 148.9, 125.7 and 106.6 mAh g^{-1} at a variable rate of 0.5, 1, 2, 5 and 10C, respectively, and then easily return to 175 mAh g^{-1} at 1C. It is a surprise that the initial capacity is 90.9 mAh g^{-1} at 10C, and 97.7% is retained after 1000 cycles. Thus, we believe that the nanocrystalline-Li_2FeSiO_4 with carbon frameworks, possessing high-capacity and high-rate performance, is promising next-generation cathode materials for high-power lithium-ion batteries.

Introduction

Recently, the Li_2MSiO_4 (M = Mn and Fe, etc.), as a new group of electrochemically active silicate-based materials for lithium ion batteries, has been attracted due to excellent chemical stability and safety imparted by the covalently bonded SiO_4 groups[1, 2], nontoxic, inexpensive materials, and insertion/ extraction two lithium per formula unit[3-9] which allows a larger theoretical specific capacity than the conventional $LiFePO_4$ cathode material. Among them, lithium iron silicate (Li_2FeSiO_4) has drawn the most attention due to its stable cycle capacity[10-12]. However, the real specific capacity with more than one Li-ion storages (>166 mAh g^{-1}) is hard to achieve, and its low rate performance is difficult to meet the requirements of high-power Li-ion batteries. One of the most key limitations is mainly attributed to its extremely low electronic conductivity. Numerous approaches have been investigated to circumvent this main issue by ameliorating the intrinsic and extrinsic properties of Li_2FeSiO_4, including porous nanostructure designing[9], supervalent or isovalent cation doping in crystals[13,14], typical carbon coating or fabrication of carbonaceous matrices[9,15], and introduction of conductive inorganic compounds[16] or organic polymers[7]. It is also suggested that emphases should be placed on lithium ion diffusion kinetics and the direct aspect related to superior high-power electrochemical properties[6,10]. It has been widely demonstrated that electrode nano-materials are significant importance to overcome such main drawback due to higher electrode/electrolyte surface contact, lesser mechanical strain upon lithium insertion/extraction from the lattice, and reduced path lengths of lithium-ion/electron transport within electrode nano-materials[17-20]. Only the improvements of both the Li-ion transport and electronic conductivity might allow Li_2FeSiO_4 cathodes have excellent specific and rate capacity properties.

It is generally known that the carbon coating can improve electronic conductivity and suppress the phase transition to increase the structural stability. Also, the carbon coating can decrease the disorder of cations in crystal sites and the transition metal dissolution, and act as a HF scavenger to reduce the electrolyte acidity[21-23]. Further, if the carbons are designed as three-dimensional (3D) conducting frameworks, not only a better electrical transport than that from the common carbon coating can be obtained[8], but also the Li-ion diffusion rate can be greatly enhanced by confining the growth of Li_2FeSiO_4 particles at nanometer-scale in synthesis and permit a fast Li-ion migration in its special porous structure. So we believe that the 3D carbon framework can effectively improve the electrochemical performance of electrode materials suffering from limited kinetics of lithium storage. Especially, it can also serve as an effective matrix for dispersing the nano-materials to prevent them from agglomerating[4,6] and then alleviate the stress and volume changes that occur in active nano-materials during the radical Li insertion/extraction process[24]. Therefore, the high specific capacity, long cyclic stability as well as the excellent high-rate performance is expected to be achieved by constituting the nanocrystalline-Li_2FeSiO_4 with carbon frameworks (NLFS-CF).

In this work, we synthesized the $P2_1/n$ structure nanocrystalline-Li_2FeSiO_4 confined with conductive carbon frameworks, which was prepared using as-prepared Li_2FeSiO_4 by hydrothermal synthesis and combining with organic polymer frameworks through a simple chelating reaction. Its formed mechanism, structure characteristics and electrochemical performance were investigated in detail. The result showed that, benefit of well-off Li-ion/electron transport capabilities, a high specific capacity with more than one Li-ion storages and stable

Cite this: DOI: 10.1039/c0xx00000x

www.rsc.org/xxxxxx

PAPER

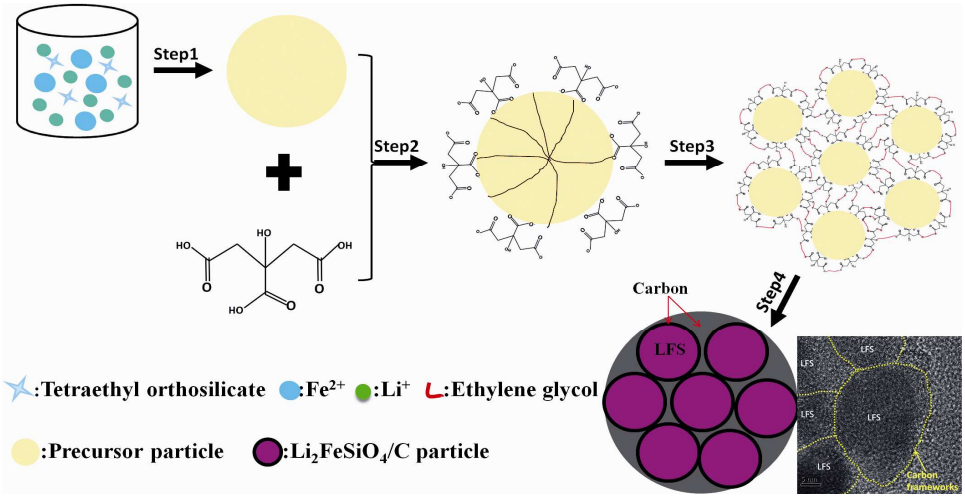

Fig. 1 Synthesis schemes of nanocrystalline-Li_2FeSiO_4 with carbon frameworks.

high-rate performance were obtained for the nanocomposite.

Experimental

Materials and Synthesis

All chemicals used were analytical grade (purchased from the Sinopharm Chemical Reagent Co., Ltd), and employed directly without any purification. The as-prepared Li_2FeSiO_4 bulk was synthesized via hydrothermal method. Firstly, 0.0125 mol of $Fe(CH_3COO)_2{\cdot}4H_2O$ was thoroughly dissolved in 10mL Ethylene glycol, and then 50mL deionized water solution with 0.0125 mol of tetraethyl orthosilicate (TEOS) and 0.05mol of $LiOH{\cdot}2H_2O$ was rapidly added. Under vigorous stirring for about 10 min, the mixture was transferred into 100 mL of Teflon-lined stainless steel autoclave and maintained at 180 ℃ for 12h. The resultant grayish precipitation was collected, washed by water and ethanol for several times, and dried at 80 ℃ in vacuum for 12 h. The obtained dry powders were added into citric acid solution and stirred for 6 h, and subsequently ethylene glycol (molar ratio of as-prepared Li_2FeSiO_4, ethylene glycol and citric acid was 1:1:1) was added and maintained 60 ℃ for 2 h. After evaporating to dryness, the mixture was pressed into pellets. The pellets were heated in a horizontal tube oven and calcinated at 650 ℃ for 10 h under a fixed nitrogen flux to obtain the nanocrystalline-Li_2FeSiO_4 with conductive carbon frameworks.

Materials characterizations

Morphologies of the samples were investigated using field emission scanning electron microscope (FE-SEM, Hitachi S-4800, 10 kV), and high-resolution transmission electron microscopy (HRTEM, JEM-2100F, 200 kV). Chemical composition was analyzed by energy dispersive X-ray spectroscopy (EDX, Horbia EX-250, 20 kV) associated with FE-SEM and Fourier transformed infrared spectroscopy (FTIR, Nicolet Avatar 360). The crystalline structure of the as-prepared samples were studied by, X-ray diffraction (XRD, D / MAX-IIIA, Cu Kα radiation, λ = 0.15406 nm, 10°/min). The carbon content in the composite was determined by thermogravimetric analysis (TG) carried out on a Netzsch STA 449C thermal analyzer. The Raman spectra were obtained by using a RM-1000 Renishaw confocal Raman microspectroscope with 514.5 nm laser radiation at a laser power of 0.04 mW in the range of 100-2000 cm^{-1}. The valence state of the key elements in samples was studied by X-ray photoelectron spectroscopy (XPS, PHI Quantera, U-P). The Fe^{4+} in the electrode at 4.5V was revealed using a Mösbauer spectrometer working with ^{57}Co as radiation source and R_h as supporter.

Electrochemical measurements

Electrochemical properties of the NLFS-CF were measured with 2032 coin cells assembled in a glove box filled with pure argon gas. Lithium pellet was used as the anode, Celgard 2400 as the separator and 1 M $LiPF_6$/EC and DMC (1:1 by volume) as the electrolyte. The working electrodes were made from a mixture of 75 wt% of the active material (NLFS-CF), 15 wt% of the conducting agent (Vulcan XC-72, Cabot), and 10 wt% of the poly(tetrafluoroethylene) (PTFE) binder. Galvanostatic charge/discharge measurement was performed in the potential range from 1.5 to 4.8 V vs Li/Li^+ with a multichannel battery testing system (LAND CT2001A) at room temperature of 30 ℃. Electrochemical impedance spectrum (EIS) was tested with an electrochemical workstation (CHI 760D).

Results and discussion

At least four steps formation mechanisms of the NLFS-CF composite can be proposed (**Fig. 1**). **Step 1:** The raw materials of $Fe(CH_3COO)_2{\cdot}4H_2O$, TEOS and $LiOH{\cdot}2H_2O$ form the as-

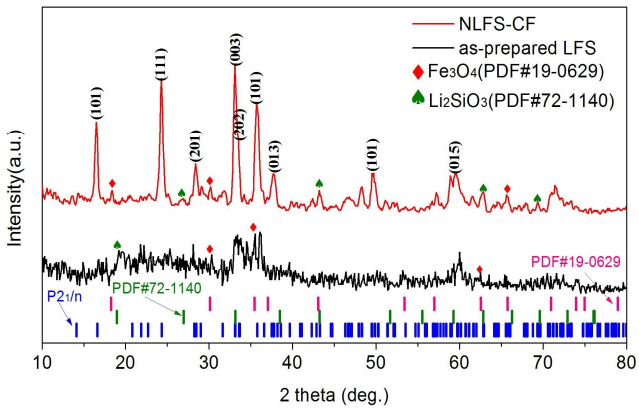

Fig. 2 XRD patterns of as-prepared Li_2FeSiO_4 and nanocrystalline-Li_2FeSiO_4 with carbon frameworks (NLFS-CF).

prepared Li_2FeSiO_4 through the hydrothermal method at 180 ℃ for 12h by reaction (1). **Step 2:** The as-prepared Li_2FeSiO_4 is dissolved to nanoscale particles in the acidic environment and coated by citric acid. **Step 3:** the organic polymer framework on the surface of the nanoparticles are formed by the adding ethylene glycol as chelating agent by reaction (2).

$$Si(OC_2H_5)_4 + 4LiOH + Fe(CH_3COO)_2 \longrightarrow Li_2FeSiO_4 + 2CH_3COOLi + 4C_2H_5OH \quad (1)$$

$$nC_6H_8O_7 + nHOCH_2CH_2OH \longrightarrow (-C_6H_7O_6\text{-}O\text{-}CH_2CH_2O\text{-})_n + nH_2O \quad (2)$$

$$Li_2FeSiO_4 + (-C_6H_7O_6\text{-}O\text{-}CH_2CH_2O\text{-})_n \longrightarrow \text{Nanocrystalline-}Li_2FeSiO_4/C \quad (3)$$

Step 4: After heat treatment the NLFS-CF appear by reaction (3), where the continuous conductive carbon frameworks enhance the electronic conductivity of the composite. Meanwhile, the formed nanocrystaline Li_2FeSiO_4 can provide a short path length for lithium ion diffusion, which facilitates the kinetics of Li_2FeSiO_4 to achieve high cyclic stability and excellent rate capability.

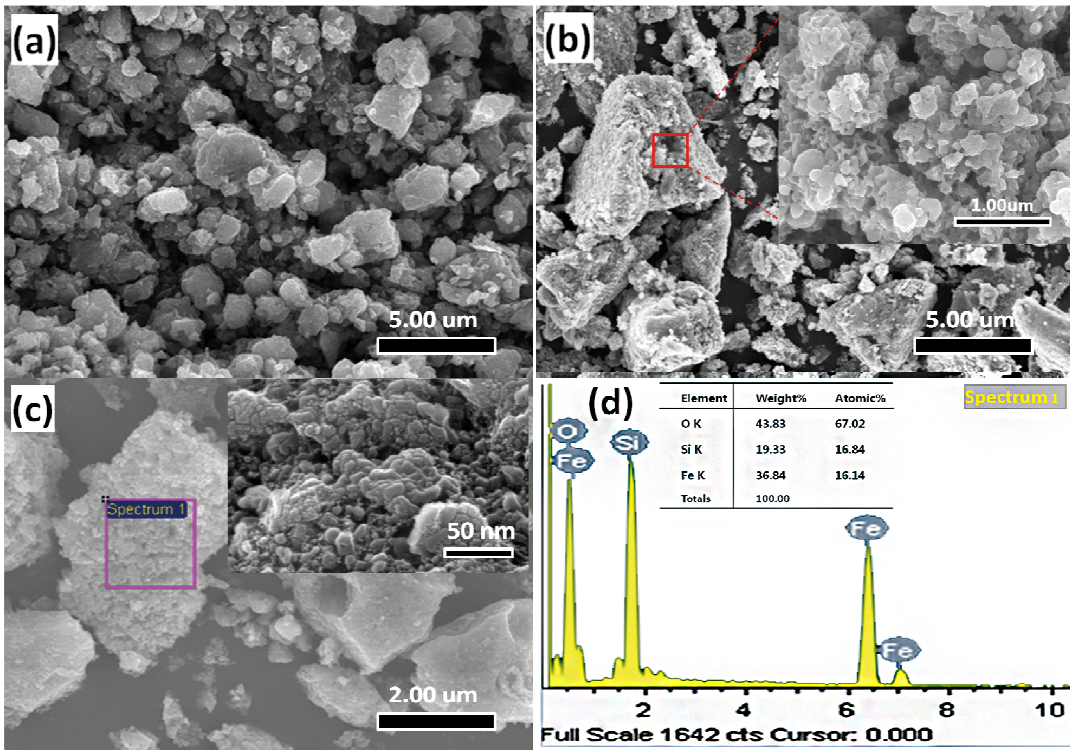

Fig. 3 SEM images of (a) as-prepared Li_2FeSiO_4 and (b, c) nanocrystalline-Li_2FeSiO_4 with carbon frameworks, (d) EDX spectra of nanocrystalline-Li_2FeSiO_4 with carbon frameworks.

Fig. 2 shows the XRD patterns of the as-prepared Li_2FeSiO_4 and the NLFS-CF composite. The as-prepared Li_2FeSiO_4 obtained after hydrothermal reaction reveals an orthorhombic structural Li_2FeSiO_4.[3] However, the peaks are not well-defined, indicating incomplete formation of Li_2FeSiO_4. After heat treating at 650 ℃ for 10 h, the prepared micro-block composite shows a highly crystalline nature, and its diffraction peaks can be indexed according to the monoclinic structure consisting with the previous reports (S.G. $P2_1/n$, a = 0.823 nm, b = 0.502 nm, c = 0.823 nm, and β= 99.2027°)[2,5]. In addition, a very little Fe_3O_4 (PDF#19-0629) and Li_2SiO_3 (PDF#72-1140) impurity are present in the both samples. Meanwhile, there is no obvious carbon peaks due to low content or amorphous state. The carbon frameworks, generated from citric acid clathrate, can be acted as conductive belts attached to nanocrystallines to promote electron transport.

Morphologies of the as-prepared Li_2FeSiO_4 and the composite after heating were investigated by FE-SEM**. Fig. 3a** exhibits a number of ~2 um Li_2FeSiO_4 blocks formed through hydrothermal

Cite this: DOI: 10.1039/c0xx00000x

www.rsc.org/xxxxxx

PAPER

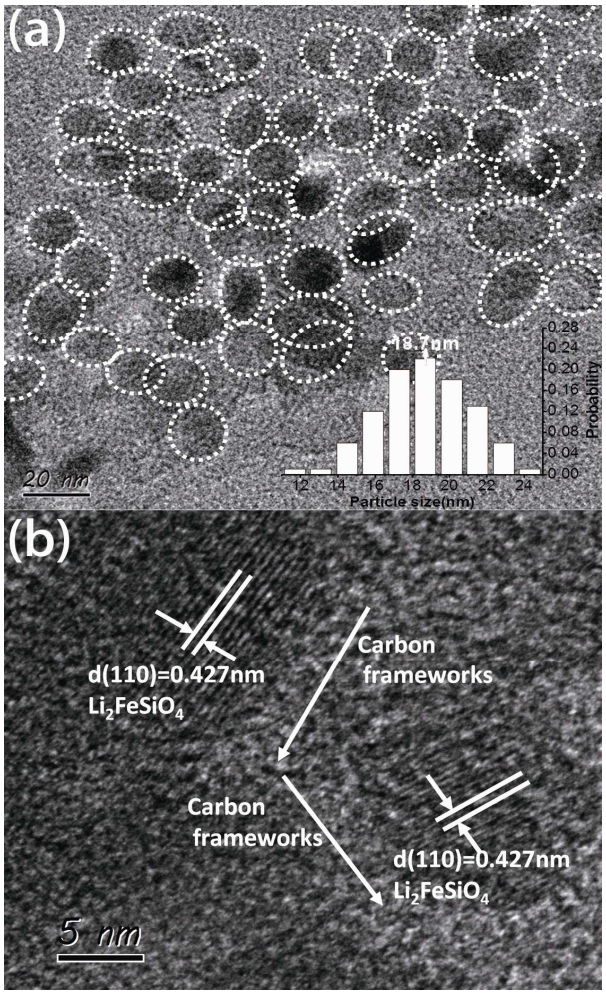

Fig. 4 (a) TEM images (inset is particle size distribution) and (b) HRTEM images of nanocrystalline-Li_2FeSiO_4 with carbon frameworks (white loops indicate nanocrystallines).

reaction. After coating by the organic polymer frameworks with heat treatment, the micro-sized composites (**Fig. 3b**) are found to be polyporous (inset of **Fig. 3b**), indicating a facilitation of electrolyte penetration. Numerous 10-20 nm Li_2FeSiO_4 particles are embedded into the carbon framework (inset of **Fig. 3c)** which can provide a large number of electronic and ionic transport channels. EDX spectrum (**Fig. 3d)** from the marked area in **Fig. 3c** shows that the atomic ratio of Fe/ Si/ O is approximately 16.14 / 16.84 / 67.02, which is close to the ratio of Fe/ Si/ O in Li_2FeSiO_4 formula. **Fig. 4a** further discloses the non-aggregated spherical morphology of Li_2FeSiO_4 nanoparticles with 10-25 nm in diameter. The particle size determined using the Scherrer formula[25] is approximately 18.3 nm, which is in good agreement with the particle size of around 18.7 nm obtained from HRTEM images by measuring more than 100 particles (inset of **Fig. 4**a). **Fig. 4b** further confirms the presence of abundant 3D carbon frameworks as matrices of Li_2FeSiO_4 nanocrystallines where the

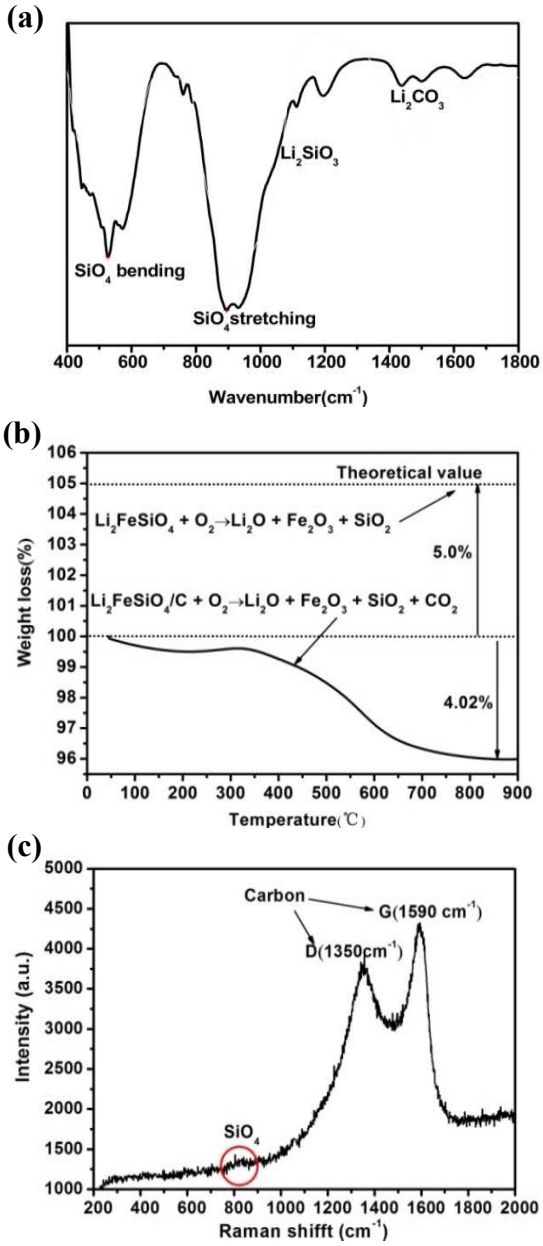

Fig. 5 (a) FTIR spectra, (b) TG curves and (c) micro-Raman spectroscopy of nanocrystalline-Li_2FeSiO_4 with carbon frameworks.

interplanar spaces of 0.427 nm corresponds to the (110) plane of the $P2_1/n$ structure. The result indicates that the 3D carbon frameworks can significantly confine the growth of Li_2FeSiO_4 particles at nanoscale during heat treatment by effectively preventing them from aggregations. The formed nanocrystalline Li_2FeSiO_4 can shorten path length of Li-ion transport and simultaneously electric conductivity can be greatly improved due to the formation of carbon frameworks. As results it can allow the NLFS-CF own an enhanced electrochemical performance.

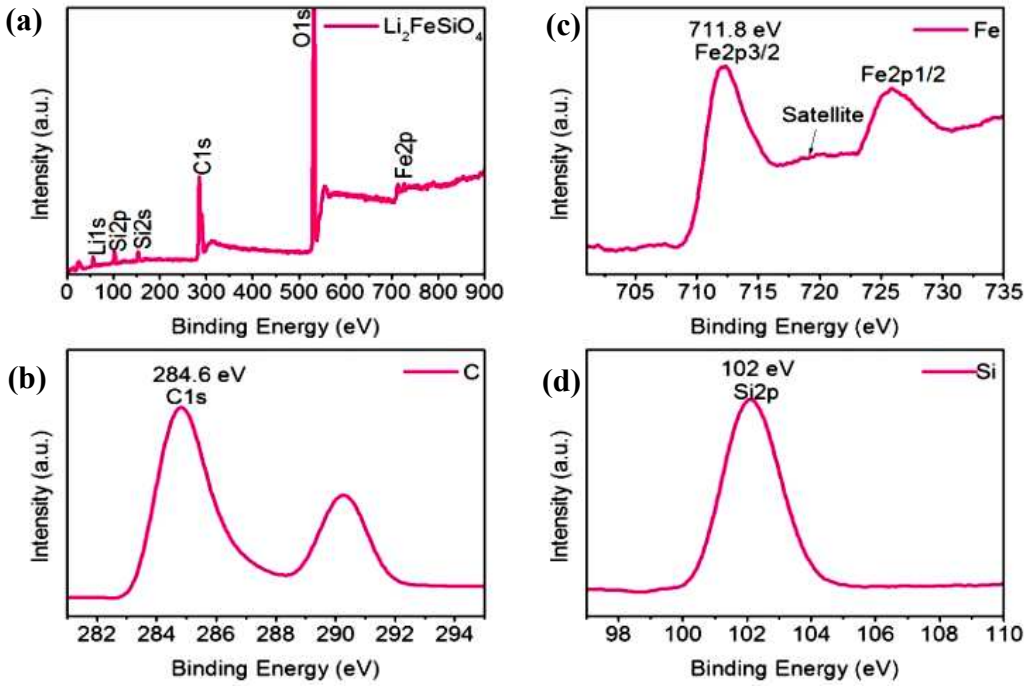

Fig. 6 XPS of nanocrystalline-Li_2FeSiO_4 with carbon frameworks.

To further investigate the material structure of the NLFS-CF, FTIR measurements were carried out. The IR vibrational spectra of Li_2FeSiO_4 are dominated by the fundamental vibrations of the LiO_4, FeO_4 and SiO_4 tetrahedral (**Fig. 5a)**, where the bending (890/977 cm^{-1}) and stretching (530/574 cm^{-1}) modes can be attributed to Si-O vibration in SiO_4 tetrahedral[26]. The bands at 1048 and 1086 cm^{-1} can be ascribed to the Si-O vibration in Li_2SiO_3, and the bands at 1442 and 1505 cm^{-1} correspond to C-O vibration in Li_2CO_3 owing to exposure in air [27, 28].

The amount of carbon released from the samples was measured using TG method (**Fig. 5b**) within a temperature range of room temperature to 900 ℃ under O_2 flow[6]. The oxidation of samples under O_2 can be carried out on the basis of following reaction

$$Li_2FeSiO_4/C + O_2 \longrightarrow Li_2O + Fe_2O_3 + SiO_2 + CO_2 \quad (4)$$

According to the theoretical calculation from reaction (4), the pure Li_2FeSiO_4 suffered from a weight increase from 100 wt% to 105 wt%[6]. So according to the results of TG analysis, the carbon content (=105 wt% - the final percentage weight) in the NLFS-CF is approximately 9 %. Micro-Raman spectroscopy was used to additional insight into the nature of composites (**Fig. 5c).** It is found that two intense broad peaks located at ~1350 and ~1590 cm^{-1} dominate typical spectra of pyrolysis carbon in the composites. The structure at 1590 cm^{-1} mainly corresponds to the G line associated with the optically allowed E_{2g} zone of crystalline graphite, and the peak at 1350 cm^{-1} mainly corresponds to the D line associated with disorder-allowed zone-edge modes of graphite[5, 26]. The calculated integrated Raman intensity ratio of I_D/I_G peaks is 0.87 (3716.219/4255.786), indicative of the presence of larger amount of graphitized carbon. Moreover, the weak Raman signal for the SiO_4 anions is identified, implying that Li_2FeSiO_4 materials were embedded in inside of the graphitized carbon frameworks.

XPS (**Fig. 6)** was further to demonstrate the structure and purity of the sample via the key element (Fe, C, and Si) analyses. **Fig. 6a** shows the XPS full-spectra of the Li_2FeSiO_4/C composite. The scale of the binding energy (BE) in XPS spectra (**Fig. 6b**) is referenced by setting the BE of C1s to 284.6 eV. The BE of Fe $2p_{2/3}$ (711.8 eV) (**Fig. 6c**) is consistent with that of ferrous ion [7], confirming the divalent state of iron in the sample. The BE of Si 2p (102 eV) (**Fig. 5d**) is in line with that of Si^{4+} in polysiloxane, indicating the formation of the [SiO_4] orthosilicate structure [7].

Galvanostatic charge-discharge measurements were carried out with lithium coin cells at a current density of 16 mA g^{-1} (0.1C) in a voltage range 1.5-4.8 V to evaluate the capacities performance of the cathode. **Fig. 7a** shows the initial two charge-discharge profiles of the sample. It can be seen that the first discharge specific capacity is 211.3 mAh g^{-1} at 0.1 C, correspond to 1.28 Li-ion storages in Li_2FeSiO_4. And the initial charge curve shows two obvious voltage platforms at approximately 3.0 and > 4.0 V. The charge curve of the subsequent second cycle presents largely difference from the first cycle. This phenomenon is ascribed to structural rearrangements involving the exchange of lithium and iron between their sites during first charge[9,29]. However, the second cycle exhibits an improved coulombic efficiency implying a more stable structure for Li-ion storage. **Fig. 7b** presents the cycle performance of the sample electrodes at 0.1C within 20 cycles. It is well known that the Li_2FeSiO_4 can gives rise to the reversible one lithium-ion extraction/insertion according to the following reactions[1, 9]:

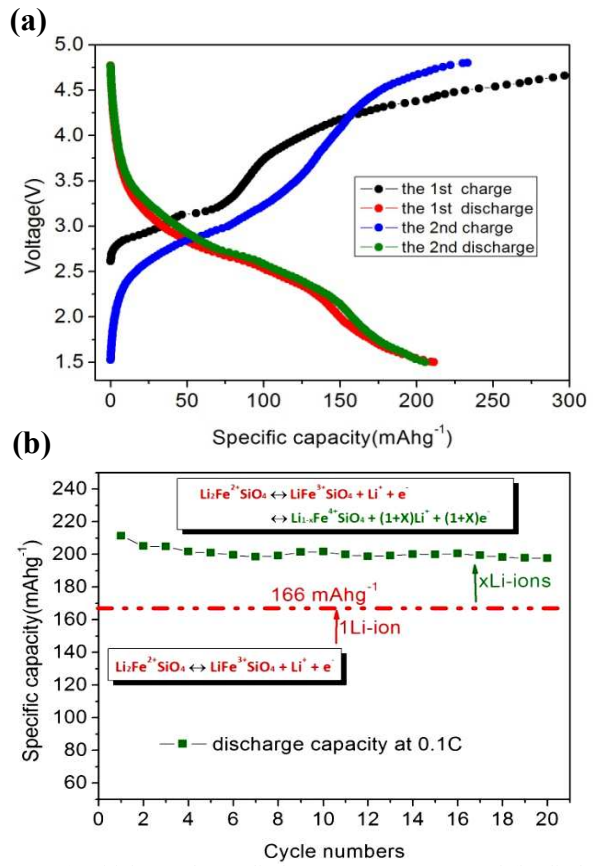

Fig. 7 (a) Initial two charge-discharge curves at 0.1C and (b) discharge capacity within 20 cycles of nanocrystalline-Li_2FeSiO_4 with carbon frameworks.

$$Li_2Fe^{2+}SiO_4 \leftrightarrow LiFe^{3+}SiO_4 + Li^+ + e^- \quad (5)$$

The second Li-ion extraction from Li_2FeSiO_4 crystal seems to be difficult because of the almost impossible successive oxidated process from Fe^{2+} though Fe^{3+} to Fe^{4+}. However, it is interesting to note that the sample exhibits high discharge capacity with more than one Li-ion storages and 100-95% capacity retention within 20 cycles at 0.1C, indicating a good stable performance. According to current reports, the high specific capacity can be caused by three reactions: (1) the reversible extraction/insertion reaction of second lithium from Li_2FeSiO_4 crystal [9]; (2) the side reaction from the decomposition of $LiPF_6$ in electrolyte [26]; (3) the irreversible extraction reaction of both Li and O (Li_2O) as a result of oxidation oxide ion from Li_2FeSiO_4 crystal [9].

In order to reveal the high capacity mechanism of the sample, the differential capacities (dQ/dV) vs. voltage plots of charge-discharge curves (**Fig. 8a**) were carried out. It can be seen that there are three charge peaks at 2.85, 3.2 and ~4.5 V, and a main discharge peak at 2.7 V with acromion occur at the first cycle. The peaks at 2.85 and 3.2 V are considered as structural rearrangements from initial $P2_1/n$-structure to cycled $Pmn2_1$-structure involving oxidation from Fe^{2+} to Fe^{3+}. The unusual peak at high potential of ~4.5 V is considered to cause the high specific capacity. It is well known that the decomposition of $LiPF_6$ and the irreversible extraction reaction of Li_2O can lead to the rapid capacity decline and the high voltage peak disappearance at subsequent cycles. However, the high reversible capacity and the peak at ~4.5V still remained at 2nd cyclic differential capacities (dQ/dV) curves indicate that the charge peak at high potential of ~4.5V is attributed to the second step oxidation[9] of Fe^{3+}/Fe^{4+}, which is further supported by ^{57}Fe Mössbauer spectra[4] of the electrode at 4.5V (inside of **Fig. 8a**), where the ratio of Fe^{4+} to Fe^{3+} is approximately 40%. The reversible reaction of more than one Li-ion extraction/insertion from Li_2FeSiO_4 is given as the following reactions[1,9]:

$$Li_2Fe^{2+}SiO_4 \leftrightarrow LiFe^{3+}SiO_4 + Li^+ + e^-$$

$$\leftrightarrow Li_{1-x}Fe^{4+}SiO_4 + (1+x)\,Li^+ + (1+x)\,e^- ;\ (x\leq 1) \quad (6)$$

In addition, as can be seen in **Fig. 8a**, the peak at 2.85V increases while the peak at 3.2V gradually decreases till disappears. This causes the distance between the charge peaks and discharge peaks is 0.15V, which is smaller than that (0.5V) in the first cycle, indicating a smaller polarization contributed by improvement of diffusion kinetics with structural rearrangements.

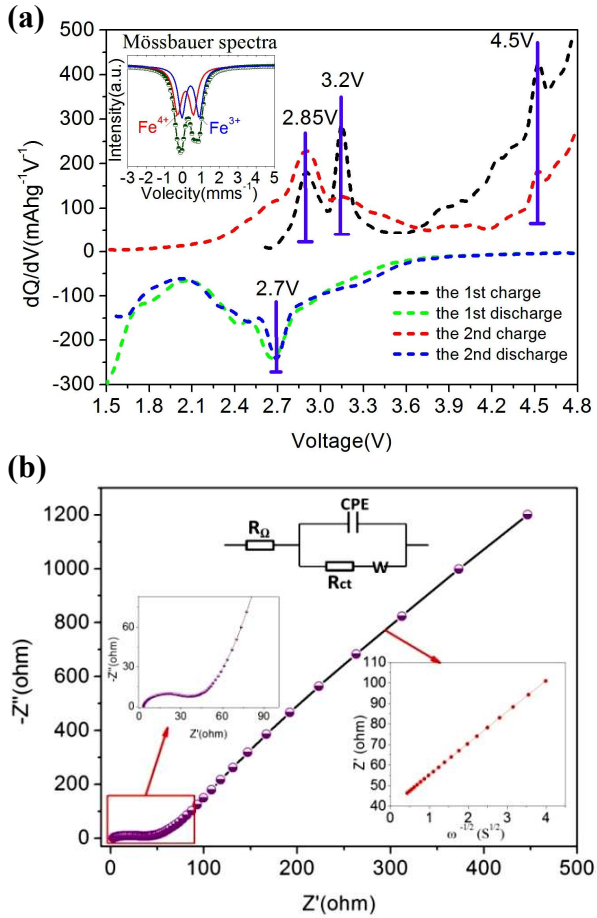

Fig. 8 (a) Differential capacities (dQ/dV) vs voltage plots of initial two charge-discharge curves (inset is ^{57}Fe Mössbauer spectra) and (b) Nyquist plots at full discharge state for the nanocrystalline-Li_2FeSiO_4 with carbon frameworks electrode. Inset of (b) shows the equivalent circuit (top), arc line in high frequency (right), linear relationship between Z' and $\omega^{-1/2}$ in low frequency region (left).

Table 1 particle Size, EIS parameters and specific capacity of Li_2FeSiO_4.

Samples	Size (nm)	D_{Li}^+ (cm^2s^{-1})	δ(scm^{-1}) /R_{ct}(Ω)	Capacity($mAhg^{-1}$) [C-rate(C)]
$Li_2FeSi_{0.9}V_{0.1}O_4/C$[14]	100-200	$6.91*10^{-14}$	-----/100	159[1/16C]
$Li_2Fe_{0.93}Zn_{0.03}SiO_4/C$[13]	100	$8.62*10^{-14}$	----/----	160[1/16C]
Li_2FeSiO_4/C/CNS[30]	57	$1.06*10^{-11}$	$5.7*10^{-4}$/123	163.8[0.1C]
Li_2FeSiO_4/RGO[31]	50	$2.40*10^{-11}$	$1.5*10^{-3}$/25.1	188/90[0.1/10C]
Li_2FeSiO_4/C[15]	31.8	$1.46*10^{-12}$	$4.9*10^{-4}$/----	177/110[0.2/5C]
This work	18.7	$6.10*10^{-10}$	$8.6*10^{-4}$/30	211/106[0.1/10C]
Li_2FeSiO_4nanosheets[7]	~1	------	----/----	340[0.02C]

To further evaluate the contribution of the interface contacts to the transport kinetics, the impedance spectra of sample were measured under fully discharged state. As shown in **Fig. 8b,** the Nyquist plot for the NLFS-CF is composed of a high-frequency semicircle and a low-frequency tail associated with the diffusion process of lithium ions in cathode (a Warburg region). The high frequency intercept on the real axis represents an ohmic resistance (R_Ω) of total resistances of the electrolyte, separator and electrical contacts. The high-frequency arc is attributed to a charge transfer resistance (R_{ct}). The inclined line at the low frequency is the Warburg impedance (Z_w), which is associated with lithium ion diffusion in the cathode active particles[14, 26].The diffusion coefficient of lithium ions (D_{Li}^+) can be calculated from the low-frequency line according to the following equation[26]:

$$D_{Li}^+ = R^2T^2/2A^2n^4F^4C^2\delta^2 \quad (7)$$

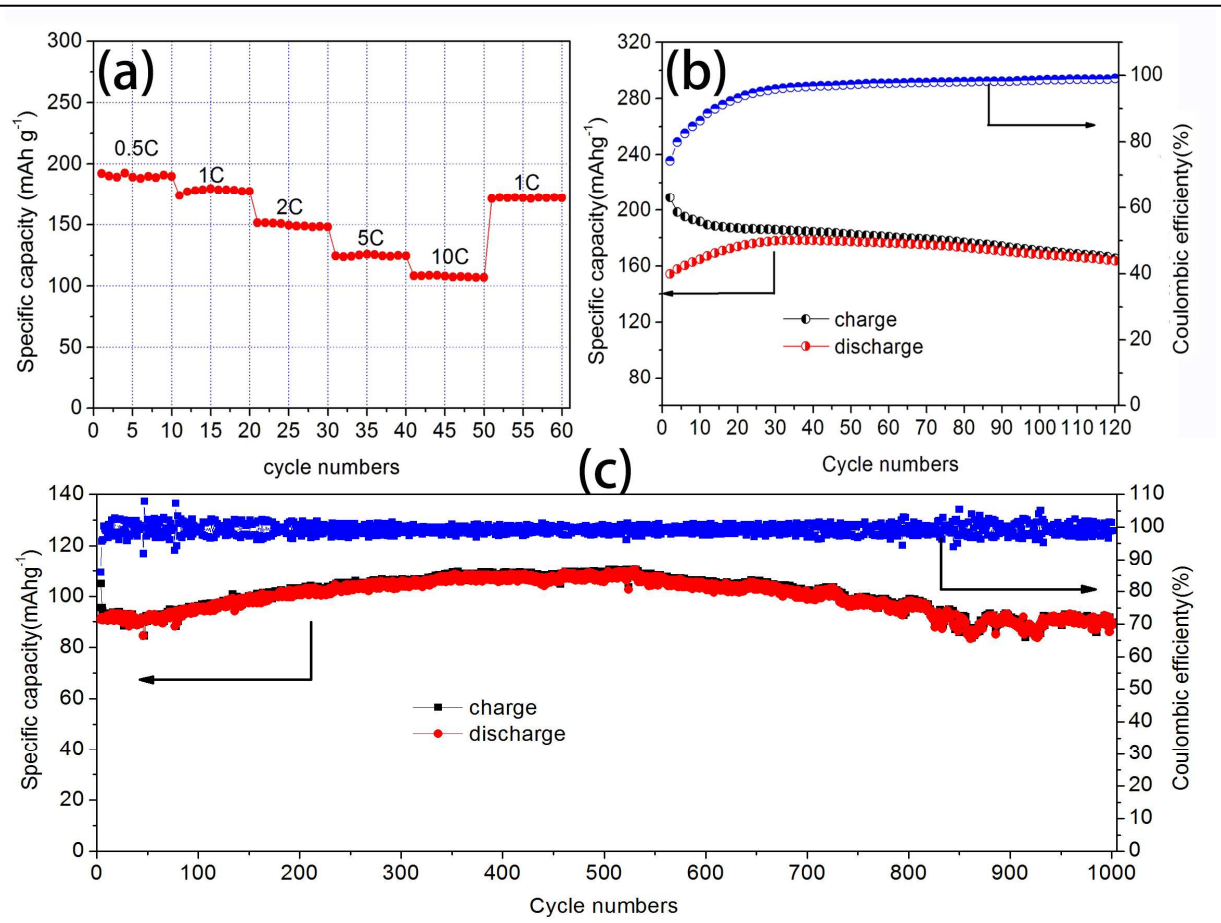

Fig. 9 (a) Rate capacities, (b) cycle performances at 1C for 120 cycles and (c) coulombic efficiency and specific reversible capacity versus cycle number for NLFS-CF at 10 C for 1000 cycles.

where R is the gas constant, T the absolute temperature, A the surface area of the electrode, n the number of electrons per molecule, F the Faraday constant, C the concentration of Li-ion, ω the angular frequency, and κ the Warburg factor to be determined from the slope of the following equation[26]:

$$Z' = B + \kappa\omega^{-1/2} \quad (8)$$

The equivalent circuit (top), arc line in high frequency (right), linear relationship between Z' and $\omega^{-1/2}$ in low frequency region (left) are shown at inset of **Fig. 8b**, respectively. A small R_{ct} (30 Ω) value corresponds to a electron conductivity (**δ**) of $8.6*10^{-4}$ s cm^{-1} and a large Li-ion diffusion coefficient (D_{Li}^+) of $6.10*10^{-10}$ cm^2 s^{-1}. **Table 1** exhibits the crystal size, D_{Li}^+, **δ** as well as the specific capacity as reported. It can be seen that the metal-ion (V, Zn, etc.) doping Li_2FeSiO_4 crystal is hard to obtain more than one Li-ion storages due to large size (≥ 100 nm) particles. However, when the size decreases to 50 nm, the capacities with over one Li-ion extraction/insertion can be achieved.. In addition, almost the electrodes possess an order of magnitude improvement of Li-ion diffusion coefficient (≥$1*10^{-12}$ cm^2 s^{-1}) and electron conductivity (or distinct reduction of R_{ct}). Among them, our NLFS-CF composite possesses excellent capacity and high-rate

performance apart from Li_2FeSiO_4 nanosheets [7].

Fig. 9a gives the specific capacity of the NLFS-CF electrodes at different C-rates. It can be seen that the discharge capacities at a variable rate of 0.5, 1, 2, 5 and 10 C are 189.8, 175.6, 148.9, 125.7 and 106.6 mAh g^{-1}, respectively, and then easily return to 175.0 mAh g^{-1} at 1C, indicating this novel material can meet the requirements of high-power Li-ion batteries. **Fig. 9b** further reveals the cyclic performance of the composite electrode at a higher C-rate of 1C (160 mA g^{-1}). The discharge capacity increases within 30 cycles mainly due to the electrolyte gradual infiltration into the porous electrodes composed of the NLFS-CF. The maximum discharge specific capacity is 176.5 mAh g^{-1} at the 30th cycle. And after 120 cycles its discharge specific capacity still maintains at 163.6 mAh g^{-1}. The long-term high rate cycling stability of the NLFS-CF was further studied at 10C rate. As plotted in **Fig. 9c**, the initial discharge capacity was 90.9 mAh g^{-1}, and 97.7% of this value was still retained after 1000 cycles. Moreover, the coulombic efficiency per cycle is up to 100%, which is predominantly attributed to convenient Li-ion and electron transport. The excellent cycle performance is due to the nanocrystalline-Li_2FeSiO_4 architecture that improves the chemical and electrochemical stability and to the presence of carbon frameworks which prevent the agglomeration of the nanocrystalline-Li_2FeSiO_4. Therefore, the unique composite material consists of nanocrystalline-Li_2FeSiO_4 and 3D carbon frameworks, with high specific capacity and long cyclic stabilities and excellent high-rate performance, is very suited to an alternative cathode material for high-power Li-ion batteries.

Conclusions

We synthesized the nanocrystalline-Li_2FeSiO_4 with conductive carbon frameworks using embedding as-prepared Li_2FeSiO_4, from hydrothermal synthesis into the carbon frameworks derived from the organic polymer frameworks by chelating reactions with citric acid and ethylene glycol and subsequently heat treating. The formed mechanism was clarified, and its structure was also characterized using XRD, SEM, HRTEM, TG, FTIR, Raman as well as XPS and ^{57}Fe Mössbauer spectra. Its electrochemical properties were investigated, by means of an enhanced electronic conductivity ($8.6*10^{-4}$ s cm^{-1}) and an improved lithium-ion diffusion coefficients ($6.10*10^{-10}$ cm^2 s^{-1}), the sample shows 1.28 Li-ion storage capacity (211.3 mAh g^{-1}) at 0.1C. Furthermore, long cyclic stabilities and excellent high-rate performances were achieved. Therefore, the new composite presents a very promising application scenario in cathode materials for power lithium-ion batteries.

Acknowledgements

This work was supported by the National Natural Science Foundation of China (NSFC) (No. 51372186).

References

1 M. E. Arroyo-de Dompablo, M. Armand, J. M. Tarascon and U. Amador, Electrochem. Commun., 2006, 8, 1292.
2 S. Nishimura, S. Hayase, R. Kanno, M. Yashima, N. Nakayama and A. Yamada, J. Am. Chem. Soc., 2008, 130, 13212.
3 T. Muraliganth, K. R. Stroukoff and A. Manthiram, Chem. Mater., 2010, 22, 5754.
4 D. Lv, W. Wen, X. Huang, J. Bai, J. Mi, S. Wu and Y. Yang, J. Mater. Chem., 2011, 21, 9506.
5 X. Wu, X. Jiang, Q. Huo and Y. Zhang, Electrochem. Acta, 2012, 80, 50.
6 Y. Zhao, J. Li, N. Wang, C. Wu, Y. Ding and L. Guan, J. Mater. Chem., 2012, 22, 18797.
7 D. Rangappa, K. D. Murukanahally, T. Tomai, A. Unemoto and I. Honma, Nano Lett., 2012, 12, 1146.
8 H. Gao, Z. Hu, K. Zhang, F. Cheng and J. Chen, Chem. Commun., 2013, 49, 3040.
9 Z. Chen, S. Qiu, Y. Cao, J. Qian, X. Ai, K. Xie, X. Hong and H. Yang, J. Mater. Chem. A, 2013, 1, 4988.
10 Z.L. Gong, Y.X. Li, G.N. He, J. Li and Y. Yang, Electrochem. Sol-Stat Lett., 2008, 11, A60.
11 A. Kojima, T. Kojima, M. Tabuchi and T. Sakai, J. Electrochem. Soc., 2012, 159, A725.
12 B. Shao and I. Taniguchi, J. Power Sources, 2012, 199, 278.
13 C. Deng, S. Zhang, S.Y. Yang, B.L. Fu and L. Ma, J. Power Sources, 2011, 196, 386.
14 H. Hao, J. Wang, J. Liu, T. Huang and A. Yu, J. Power Sources, 2012, 210, 397.
15 Z. Zheng, Y. Wang, A. Zhang, T. Zhang, F. Cheng, Z. Tao and J. Chen, J. Power Sources, 2012, 198, 229.
16 J. Bai, Z. Gong, D. Lv, Y. Li, H. Zou and Y. Yang, J. Mater. Chem., 2012, 22, 12128.
17 L. Qu, S. Fang, L. Yang and S. Hirano, J. Power Sources, 2012, 217, 243.
18 Z. Yan, S. Cai, X. Zhou, Y. Zhao and L. Miao, J. Electrochem. Soc., 2012, 159, A894.
19 K.C. Kam, T. Gustafsson and J.O. Thomas, Solid State Ionics, 2011, 192, 356.
20 D. M. Kempaiah, D. Rangappa and I. Honma, Chem. Commun., 2012, 48, 2698.
21 D. Ensling, M. Stjerndahl, A. Nytén, T. Gustafsson and J.O. Thomas, J. Mater. Chem., 2009, 19, 82.
22 H. Li and H. Zhou, Chem. Commun., 2012, 48, 1201.
23 J. Zhao, J. He, J. Zhou, Y. Guo, T. Wang, S. Wu, X. Ding, R. Huang and H. Xue, J. Phys. Chem. C, 2011, 115, 2888.
24 S. Xin, Y. Guo and L. Wan, accounts of chemical research, 2012, 45, 1759.
25 O. Toprakci, H.A.K. Toprakci, L. Ji, G. Xu, Z. Lin and X. Zhang, ACS Applied. Mater. Inter., 2012, 4, 1273.
26 R. Fu, Y. Li, H. Yang, Y. Zhang and X. Cheng, J. Electrochem. Soc., 2013, 160, A3048.
27 C. Deng, S. Zhang, Y. Gao, B. Wu, L. Ma, Y.H. Sun, B.L. Fu, Q. Wu, and F.L. Liu, Electrochem. Acta, 2011, 56, 7327.
28 B. Zhang, M. Nieuwoudt and A. J. Easteal, J. Am. Ceram. Soc., 2008, 91, 1927.
29 A. Nytén, S. Kamali, L. Häggström, T. Gustafsson and J.O. Thomas, J. Mater. Chem., 2006, 16, 2266.
30 J. Yang, X. Kang, L. Hu, X. Gong, D. He, T. Peng and S. Mu, J. Alloys Comp., 2013, 572, 158.
31 L. Zhang, S. Duan, X. Yang, G. Peng, G. Liang, Y.Huang, Y. Jiang, S. Ni and Ming Li, ACS Appl. Mater. Interfaces, 2013, DOI: 10.1021/am402434n.